CMS Physics Analysis Summary

Contact: cms-pag-conveners-susy@cern.ch 2015/12/16

Search for new physics in final states with jets and missing transverse momentum in $\sqrt{s}$ = 13 TeV pp collisions with the α_{T} variable

The CMS Collaboration

Abstract

An inclusive search for supersymmetric processes that produce final states with jets and missing transverse momentum is performed in pp collisions at a centre-of-mass energy of 13 TeV. A dimensionless kinematic variable, α_{T}, is used to discriminate between events with genuine and misreconstructed missing transverse momentum. A data sample corresponding to an integrated luminosity of 2.2 fb^{-1}, recorded by the CMS experiment at the LHC, is analysed. The observed signal candidate event counts are found to be in agreement with the expected contributions from standard model processes and the result is interpreted in the mass parameter space of supersymmetric simplified models.

1 Introduction

Supersymmetry (SUSY) [1–8] provides a complete, renormalisable extension to the Standard Model that can provide a solution to the hierarchy problem of the SM Higgs boson [9, 10] providing SUSY is realised at the TeV scale. Further, the assumption of R-parity conservation [11] has important consequences for collider phenomenology and cosmology. Supersymmetric particles (sparticles) such as gluinos and squarks are expected to be produced in pairs at the LHC and promptly decay to the lightest stable supersymmetric particle (LSP), which is generally assumed to be a weakly interacting, massive neutralino and a dark matter candidate. The characteristic signature of SUSY production at the LHC is a final state of multijets accompanied by significant missing transverse momentum, $\vec{p}_{\mathrm{T}}^{\,\mathrm{miss}}$.

The new energy frontier of the LHC during Run 2 provides a unique opportunity to search for the characteristic signatures of TeV-scale sparticles. This Physics Analysis Summary presents an inclusive search for the pair production of massive coloured sparticles in hadronic final states with two or more energetic jets and missing transverse momentum, performed in pp collisions at a centre-of-mass energy $\sqrt{s} = 13\,\mathrm{TeV}$. The analysed data sample corresponds to an integrated luminosity of $2.2 \pm 0.1\,\mathrm{fb}^{-1}$ [12] collected by the Compact Muon Solenoid (CMS) experiment. Previous iterations of this search have been performed in pp collisions at both $\sqrt{s} = 7$ [13–15] and 8 TeV [16].

The search strategy is based around two key aspects in order to achieve a robust, inclusive search capable of exploiting the potential of the new LHC energy frontier under the challenging conditions of new beam and detector configurations early in Run 2. First, multiple tight selection criteria are employed to suppress multijet production, a manifestation of quantum chromodynamics (QCD), to a negligible level relative to all other SM background processes. Second, the experimental acceptance to a potential signal is maximised through the use of trigger conditions that maintain the same low thresholds employed during Run 1.

The strategy is built around the use of the kinematic variable α_{T} [13, 17], which provides powerful discrimination against multijet production. The α_{T} variable is constructed from jet-based quantities to provide robust discriminating power between sources of genuine and misreconstructed missing transverse momentum, making it suitable for early searches operating at new energy and luminosity frontiers. The α_{T} variable is utilised as part of the trigger conditions, providing high performance in terms of maintaining low thresholds for a given trigger bandwidth. Further variables are also employed to discriminate against multijet production and suppress this background process to a negligible level. The $\Delta\phi^{*}_{\mathrm{min}}$ [13] variable exploits azimuthal angular information and also provides strong rejection power against multijet events, including rare energetic events in which neutrinos carry a significant fraction of a jet's energy due to semileptonic decays of heavy-flavour mesons.

The search is based on an examination of the number of reconstructed jets per event, the number of these jets identified as originating from bottom quarks, and the scalar and vector sums of transverse momenta of these jets. These discriminating variables provide sensitivity to the different production mechanisms of massive coloured sparticles at hadron colliders (i.e. squark-squark, squark-gluino, and gluino-gluino), third-generation squark signatures, and a large range of mass splittings between the parent sparticle and the LSP, respectively. Interpretations of the result are provided in the parameter space of simplified models [18–20] that represent the pair production of gluinos and their subsequent prompt decays to four quarks and two LSPs via off-shell squarks of light or heavy flavour, as illustrated in Fig. 1.

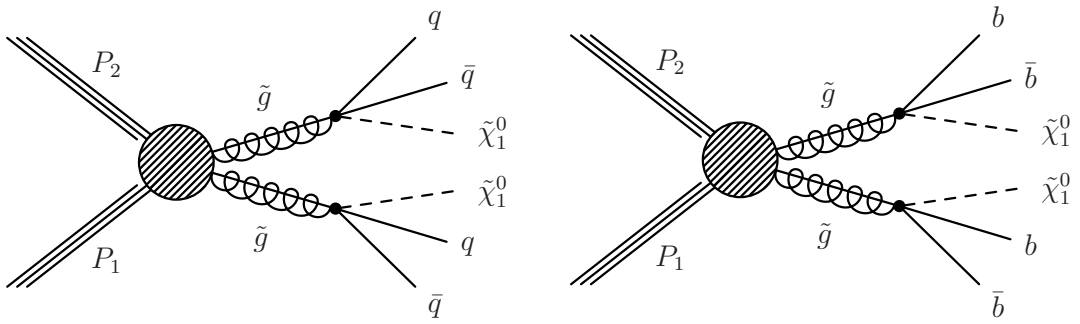

Figure 1: Representations of simplified models comprising the pair production of gluinos and prompt three-body decays to $q\bar{q}\tilde{\chi}_1^0$ (left) and $b\bar{b}\tilde{\chi}_1^0$ (right) via an off-shell light-flavour or bottom squark, respectively.

2 The CMS detector

The central feature of the CMS apparatus is a superconducting solenoid of 6 m internal diameter, providing a magnetic field of 3.8 T. Within the superconducting solenoid volume are a silicon pixel and strip tracker, a lead tungstate crystal electromagnetic calorimeter (ECAL), and a brass and scintillator hadron calorimeter (HCAL), each composed of a barrel and two endcap sections. Forward calorimeters extend the pseudorapidity [21] coverage provided by the barrel and endcap detectors. Muons are measured in gas-ionization detectors embedded in the steel flux-return yoke outside the solenoid. The missing transverse momentum vector $\vec{p}_{\mathrm{T}}^{\,\mathrm{miss}}$ is defined as the projection on the plane perpendicular to the beams of the negative vector sum of the momenta of all reconstructed particles in an event. Its magnitude is referred to as $E_{\mathrm{T}}^{\mathrm{miss}}$. A more detailed description of the CMS detector, together with a definition of the coordinate system used and the relevant kinematic variables, can be found in Ref. [21].

3 Signal candidate event selection

The event reconstruction and selection criteria described below are explained in more detail in Ref. [16]. In order to suppress SM processes with genuine $E_{\mathrm{T}}^{\mathrm{miss}}$ from neutrinos and select only multijet final states, events containing an isolated electron [22] or muon [23] with $p_{\mathrm{T}} > 10\,\mathrm{GeV}$ or isolated photon [24] with $p_{\mathrm{T}} > 25\,\mathrm{GeV}$ are vetoed. Furthermore, events containing an isolated track with $p_{\mathrm{T}} > 10\,\mathrm{GeV}$ are also vetoed in order to reduce the background contribution from final states containing hadronically-decaying tau leptons.

Jets are reconstructed using the particle-flow (PF) reconstruction algorithm [25, 26] and clustered by the anti-k_{T} algorithm [27] with a size parameter of 0.4. The jet energies are corrected to account for the effects of pileup and to establish a uniform relative response in η and a calibrated absolute response in transverse momentum p_{T} [28]. Jets considered in the analysis are required to have a transverse energy above 40 GeV and $|\eta| < 3$. The mass scale of the physics processes being probed is characterised by the scalar sum of the transverse momenta p_{T} of these jets, defined as $H_{\mathrm{T}} = \sum_{i=1}^{N_{\mathrm{jet}}} p_{\mathrm{T}}{}^{\mathrm{j}_i}$, where N_{jet} is the number of jets within the experimental acceptance. The estimator for $E_{\mathrm{T}}^{\mathrm{miss}}$ is given by the magnitude of the vector sum of the transverse momenta of these jets, defined by $H_{\mathrm{T}}^{\mathrm{miss}} = |\sum_{i=1}^{N_{\mathrm{jet}}} \vec{p}_{\mathrm{T}}^{\,\mathrm{j}_i}|$. Events are vetoed if rare, spurious signals are identified in the calorimeters [29, 30] or if any additional jet satisfies $p_{\mathrm{T}} > 40\,\mathrm{GeV}$ and $|\eta| > 3$, in order to maintain the performance of the variable $H_{\mathrm{T}}^{\mathrm{miss}}$ as an estimator of $E_{\mathrm{T}}^{\mathrm{miss}}$.

Significant hadronic activity and $E_{\mathrm{T}}^{\mathrm{miss}}$ in the event is ensured by requiring $H_{\mathrm{T}} > 200\,\mathrm{GeV}$ and $H_{\mathrm{T}}^{\mathrm{miss}} > 130\,\mathrm{GeV}$, respectively. The most energetic jet in the event is required to satisfy

$p_T > 100\,\text{GeV}$. A requirement on the second most energetic jet is used to categorise the events. If the jet satisfies $p_T > 100\,\text{GeV}$, then this category of events is labelled "symmetric" and targets primarily the topology of pair-produced sparticles. If the second most energetic jet satisfies $40 < p_T < 100\,\text{GeV}$ or $p_T < 40\,\text{GeV}$, then these categories are labelled as an "asymmetric" or "monojet" topology, respectively. The final two topologies target primarily dark matter and nearly mass-degenerate SUSY models. Events are further categorised according to the number of jets per event (n_{jet}) and the number of reconstructed jets identified as originating from a b-quark (n_b).

A number of beam- and detector-related effects can lead to events with large values of E_T^{miss}, such as beam halo, reconstruction failures, spurious detector noise, or event misreconstruction due to detector inefficiencies. These events, with large, non-physical values of E_T^{miss}, are rejected with high efficiency by applying a range of dedicated vetoes [16, 31].

Table 1: Summary of the selection criteria and categorisation used in the definitions of the signal and control regions.

Baseline selection:	
Jets selection	Select jets satisfying $p_T > 40\,\text{GeV}$ and $\lvert\eta\rvert < 3$
Forward jet veto	Veto events containing jet satisfying $p_T > 40\,\text{GeV}$ and $\lvert\eta\rvert > 3$
Lepton/photon vetoes	$p_T > 10$, 10, 25 GeV for leptons, isolated tracks, photons (respectively) and $\lvert\eta\rvert < 2.5$
Lead jet acceptance	$p_T > 100\,\text{GeV}$ and $\lvert\eta\rvert < 2.5$
Second jet acceptance	$p_T > 100\,\text{GeV}$ (symmetric), $40 < p_T < 100\,\text{GeV}$ (asymmetric), $p_T < 40\,\text{GeV}$ (monojet)
Energy sums	$H_T > 200\,\text{GeV}$ and $H_T^{\text{miss}} > 130\,\text{GeV}$
E_T^{miss} cleaning	Various filters related to beam and instrumental effects
(n_{jet},nb) categorisation and H_T binning:	
n_{jet} binning	1 (monojet), 2, 3, 4, $\geq$5 (both symmetric and asymmetric)
n_b binning	0, 1, 2, $\geq$ 3 ($n_b \leq n_{\text{jet}}$)
H_T (GeV) binning	200, 250, 300, 350, 400, 500, 600, >800 GeV (bins can be merged depending on n_{jet}, n_b)
Signal region:	
QCD suppression	$\alpha_T > 0.65$ to $\alpha_T > 0.52$ (H_T-dependent, for the region $H_T < 800\,\text{GeV}$)
QCD suppression	$\Delta\phi^*_{\text{min}} > 0.5$
QCD suppression	$H_T^{\text{miss}}/E_T^{\text{miss}} < 1.25$

For events satisfying the baseline selection criteria described above, summarised in Table 1, the multijet background dominates over all other SM backgrounds. The α_T kinematic variable, first introduced in Refs. [13, 17], is used to efficiently reject multijet events with transverse energy mismeasurements while retaining sensitivity to new physics with genuine E_T^{miss} signatures. The variable α_T depends solely on the measurements of the transverse energies and azimuthal angles of jets and it is intrinsically robust against the presence of jet energy mismeasurements in multijet systems. For dijet events, the α_T variable is defined as $\alpha_T = E_T^{j2}/M_T$ where E_T^{j2} is the transverse energy of the less-energetic jet, and M_T is the transverse mass of the dijet system. For a perfectly measured dijet event with $E_T^{j1} = E_T^{j2}$ and jets back-to-back in ϕ, and in the limit in which the momentum of each jet is large compared with its mass, the value of α_T is 0.5. For the case of an imbalance in the measured transverse energies of back-to-back jets, α_T is reduced to a value smaller than 0.5, which gives the variable its intrinsic robustness. Values significantly greater than 0.5 are observed when the two jets are not back to back and are recoiling against significant, genuine E_T^{miss}. The definition of the α_T variable can be generalised for events with two or more jets, as described in Ref. [16].

Multijet events typically populate the region $\alpha_T \lesssim 0.5$ and the α_T distribution is characterised by a sharp edge at 0.5, beyond which the multijet event yield falls by several orders of magnitude. Multijet events with extremely rare but large stochastic fluctuations in the calorimetric measurements of jet energies can lead to values of α_T slightly above 0.5. The edge at 0.5 sharp-

ens with increasing H_T for multijet events, primarily due to a corresponding increase in the average jet energy and thus an improvement in the jet energy resolution, but also because the threshold effect of jets below the p_T threshold contributing significantly to H_T^{miss} decreases with increasing H_T. This motivates a H_T-dependent α_T requirement that varies in the range 0.52–0.65 for the region $H_T > 800\,GeV$.

The $\Delta\phi^*_{min}$ variable considers the minimum azimuthal angular separation of a jet and the H_T^{miss} vector derived from all other jets in the event. The $\Delta\phi^*_{min}$ variable provides powerful discriminating power between final states with genuine E_T^{miss} and mismeasured QCD multijet events. The variable is also highly efficient at suppressing any potential contribution from rare energetic multijet events that yield high jet multiplicities and significant E_T^{miss} due to high-multiplicity neutrino production in semileptonic heavy-flavour decays. The neutrinos are typically collinear with respect to the axis of a jet and carry a significant fraction of the energy. The requirement $\Delta\phi^*_{min} > 0.5$ is sufficient to suppress effectively the multijet background.

For the region $H_T < 800\,GeV$, the requirements on both the α_T and $\Delta\phi^*_{min}$ variables are utilised, whereas for the region $H_T > 800\,GeV$, the necessary control of the QCD multijet background is achieved solely with the $\Delta\phi^*_{min}$ requirement. Figure 2 shows the α_T and $\Delta\phi^*_{min}$ distributions observed in data for events that satisfy all other signal region selection criteria plus $H_T > 300\,GeV$ and $H_T > 800\,GeV$, respectively. In the case of the α_T distribution, the events that satisfy $\alpha_T < 0.55$ must only fulfill the baseline selection criteria defined in Table 1, no H_T^{miss} requirement is made, and the events are recorded with an unbiased set of trigger H_T conditions.

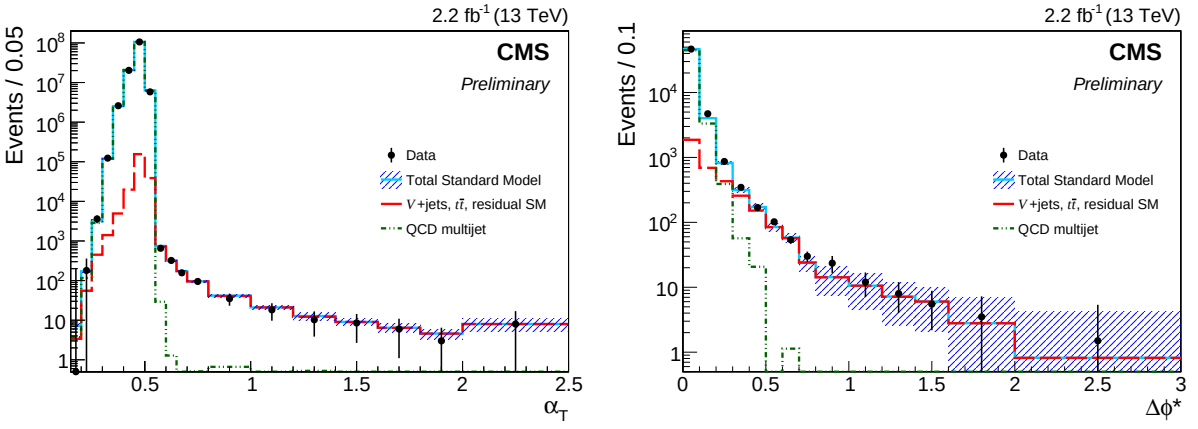

Figure 2: (Left) The α_T distribution observed in data for events that are recorded with unbiased trigger conditions and satisfy the baseline (full signal region) selection criteria for the region $\alpha_T < 0.55$ ($\alpha_T > 0.55$). (Right) The $\Delta\phi^*_{min}$ distribution observed in data for events that satisfy the full signal region selection criteria and $H_T > 800\,GeV$. The distributions for the QCD multijet backgrounds are determined from simulation while all other SM backgrounds are estimated using a μ + jets data control sample.

A final dedicated veto is employed to deal with the rare circumstance in which several jets with transverse energies below the E_T thresholds and collinear in ϕ can result in significant H_T^{miss} relative to E_T^{miss}, the latter of which is less sensitive to jet thresholds. This type of background, typical of multijet events, is suppressed while maintaining high efficiency for SM or new physics processes with genuine, significant missing transverse momentum by requiring $H_T^{miss}/E_T^{miss} < 1.25$.

The aforementioned requirements complete the definition of the signal region. Signal candidate events are recorded with multiple jet-based trigger conditions that require both H_T and α_T

to satisfy predetermined thresholds. In addition, a trigger condition based solely on H_T is used to record candidate events for the region $H_T > 800\,\text{GeV}$. A dedicated trigger condition comprising the presence of a jet and significant H_T^{miss} and E_T^{miss} is used to record monojet events. The trigger-level jet energies are corrected to account for energy scale and pileup effects. The trigger strategy provides efficiencies at or near 100% for all bins of the signal region.

Finally, the search exploits the use of the H_T^{miss} variable as a discriminant between the dominant SM backgrounds and new physics signatures. The H_T^{miss} templates are derived from simulation that are extensively validated in multiple data control regions and from which systematic uncertainties are established.

4 Background estimation for QCD multijet production

The signal region is defined such that the expected contribution from multijet events is suppressed to the percent level with respect to the total expected background counts from other SM processes for all event categories and H_T bins. This is achieved through very tight requirements on the variables α_T, $\Delta\phi^*_{min}$, and H_T^{miss}/E_T^{miss}, as described above.

Potential contamination from multijet events in the signal region is estimated by exploiting the ratio of multijet events that satisfy or fail the requirement $H_T^{miss}/E_T^{miss} < 1.25$. This ratio is determined from simulated events categorised according to n_{jet} and H_T and validated in a multijet-enriched data sideband defined by $\Delta\phi^*_{min} < 0.5$. Estimates of the QCD multijet background counts, binned according to n_{jet} and H_T, are determined in a further data sideband, defined by the requirement $H_T^{miss}/E_T^{miss} > 1.25$, by correcting the observed counts in data to account for contamination from vector boson and $t\bar{t}$ production (plus residual contributions from other SM processes). The product of the corrected counts and ratios provide an independent estimate of the QCD multijet contamination as a function of n_{jet} and H_T, with an assumed systematic uncertainty of 100% based on the validation in the multijet-enriched data sidebands. The estimates are found to negligible, typically at the percent level, relative to the sum of all other SM backgrounds in each bin across the full signal region phase space. The distribution of any residual contamination as a function of n_b and H_T^{miss} is determined from simulation. Finally, data control variables are inspected to provide confidence that any multijet contamination due to instrumental effects is negligible.

5 Background estimation for SM processes with genuine E_T^{miss}

In the absence of multijet events, the background counts in the signal region arise from SM processes with significant E_T^{miss} in the final state. In events with low counts of jets and b-quark jets, the largest backgrounds with genuine E_T^{miss} are from the associated production of W or Z bosons with jets, followed by either the weak decays $Z \to \nu\bar{\nu}$ or $W \to \tau\nu$, where the τ decays hadronically and is identified as a jet; or by leptonic decays that are not rejected by the dedicated electron or muon vetoes. The veto of events containing isolated tracks is efficient at further suppressing these backgrounds as well as the single-prong hadronic decay of the tau lepton. At higher jet and b-quark jet multiplicities, top quark production followed by semileptonic weak top quark decay becomes important.

The production of W and Z bosons in association with jets, $t\bar{t}$ and γ + jets processes are simulated with the MADGRAPH V5 [32] event generator. The production of single-top quark events is generated with POWHEG [33], and diboson events are produced with PYTHIA 8.1 [34]. For all simulated samples, PYTHIA 8.1 is used to describe parton showering and hadronisation.

All samples are generated using the CTEQ6L1 [35] parton distribution functions (PDF). The description of the detector response is implemented using the GEANT4 [36] package. The simulated samples are normalised using the most accurate cross section calculations currently available, usually with next-to-next-to-leading-order (NNLO) accuracy. To model the effects of pileup, the simulated events are generated with a nominal distribution of pp interactions per bunch crossing and then reweighted to match the pileup distribution as measured in data.

The method to estimate the non-multijet backgrounds in the signal region relies on the use of transfer factors, which are constructed per bin (in terms of n_{jet}, n_{b}, and H_{T}) per data control sample. The transfer factors are determined from the simulated event samples and are ratios of expected yields in the corresponding bins of the signal region and control samples. The transfer factors are used to extrapolate from the event yields measured in data control samples to an expectation for the total background event yields in the signal region.

Three disjoint data control regions, binned identically to the signal region, are used to estimate the contributions from the various remaining SM background processes. The control regions are defined by a selection of μ + jets, $\mu\mu$ + jets, and γ + jets events. The selection criteria are chosen such that the SM processes and their kinematic properties resemble as closely as possible the SM background behaviour in the signal region once the muon, dimuon system, or photon are ignored when computing quantities such as H_{T}, $H_{\mathrm{T}}^{\mathrm{miss}}$ and α_{T}. The baseline selection criteria and binning definition described in Table 1 are applied to all control samples, except for the lepton and photon vetoes, which are inverted and tightened to improve purity. The event selection criteria are defined to also ensure that any potential contamination from multijet events or a wide variety of SUSY models (i.e. signal contamination) is negligible.

The μ + jets sample is recorded using a trigger condition that requires an isolated muon and the event selection criteria are chosen in order to ensure high trigger efficiency. Furthermore, the muon is required to be well separated from the jets in the event and the transverse mass (M_{T}) of the muon and $E_{\mathrm{T}}^{\mathrm{miss}}$ [25, 26] system must satisfy $30 < M_{\mathrm{T}} < 125\,\mathrm{GeV}$ to ensure a sample rich in W bosons (produced promptly or from the decay of top quarks). The $\mu\mu$ + jets sample uses similar selection criteria as the μ + jets sample and the same trigger condition. Exactly two oppositely-charged, isolated muons are required, the muons must be distanced from the jets in the event, and the invariant mass of the dimuon system must be within a window of $\pm 25\,\mathrm{GeV}$ around the mass of the Z boson. For both the muon and dimuon samples, no requirement is made on the variable α_{T} in order to increase the statistical precision of the predictions derived from these samples, in constrast to the identical α_{T} requirements made for the signal region and photon control sample. The γ + jets sample is recorded using a single photon trigger condition. The event selection criteria comprise an isolated photon with $E_{\mathrm{T}} > 200\,\mathrm{GeV}$ and $H_{\mathrm{T}} > 400\,\mathrm{GeV}$.

Three independent estimates of the irreducible background of $\mathrm{Z} \to \nu\bar{\nu}$ + jets events are determined from the γ + jets, $\mu\mu$ + jets, amd μ + jets data control samples. The γ + jets and $\mathrm{Z} \to \mu\mu$ + jets processes have similar kinematic properties when the photon or muons are ignored [37], albeit different acceptances. In addition, the γ + jets process has a larger production cross section than $\mathrm{Z} \to \nu\bar{\nu}$ + jets events. The μ + jets data sample is used to provide an estimate for the $\mathrm{Z} \to \nu\bar{\nu}$ + jets contribution as well as the other dominant SM processes, $\mathrm{t\bar{t}}$ and W boson production. Residual contributions from processes such as single-top-quark, diboson, and Drell-Yan production are also included.

The uncertainty in the transfer factors derived from simulation is probed through closure tests based on data control samples [16]. Each closure test inspects the compatibility of yields in two disjoint data control samples and a corresponding transfer factor derived from simulation. A large ensemble of tests are performed to probe the simulation modelling of a range of key

Table 2: Systematic uncertainties (percent) in the estimates of the normalisation of the SM background components as a function of n_{jet}, as determined from ensembles of closure tests based on multiple data control samples. The quoted ranges correspond to the variations determined across the n_{b} and H_{T} bins of a given n_{jet} category. The additional contributions listed at the foot of the table are added in quadrature to the n_{jet}-dependent contributions for each SM background component.

n_{jet}	Uncertainty (%) in background component	
	$\bar{\text{t}}\text{t}$, W+jets, residual SM	$\text{Z} \to \nu\bar{\nu}$ + jets
"Monojet":		
1	9–36	9–36
"Asymmetric":		
2	11–105	9–46
3	12–86	12–78
4	16–52	13–43
$\geq$5	19–47	27–73
"Symmetric":		
2	7–34	11–30
3	9–31	13–44
4	13–36	8–34
$\geq$5	15–22	17–28
Additional contributions:		
α_{T} ($H_{\text{T}} < 800\,\text{GeV}$)	10-27	10-27
$\Delta\phi^{*}_{\text{min}}$ ($H_{\text{T}} > 800\,\text{GeV}$)	22	22
b-quark identification	<5	<5

physics effects that may lead to potential biases in the transfer factors [16]. For the analysed data sample, the closure tests reveal no significant biases or dependencies on n_{jet} or H_{T} for all individual tests. Systematic uncertainties in the transfer factors are typically determined from ensembles of closure tests, which can be considered as "normalisation" uncertainties for a given component of background events categorised according to n_{jet}, n_{b}, and H_{T}. Table 2 summarises typical values for the systematic uncertainties in experimental acceptance effects for the dominant SM background components. These uncertainties are assumed to be fully uncorrelated for events catogorised differently in n_{jet}, n_{b}, and H_{T}. The uncertainties associated with extrapolations in the α_{T} and $\Delta\phi^{*}_{\text{min}}$ variables, and the simulation modelling of the efficiency and mistag rates for identifying jets originating from b quarks or light-flavour partons are also listed, which are assumed to be fully correlated across the n_{b} dimension only.

Templates derived from simulation are used to predict the background counts in the $H_{\text{T}}^{\text{miss}}$ dimension. Multiple data control regions are used to evaluate the degree to which the simulation describes the $H_{\text{T}}^{\text{miss}}$ distributions observed in data, and to assign appropriate systematic uncertainties that can be in excess of $> 100\%$ in the most sensitive $H_{\text{T}}^{\text{miss}}$ bins. Independent systematic uncertainties in the templates for the $\text{Z} \to \nu\bar{\nu}$ + jets background and the W + jets and $\bar{\text{t}}\text{t}$ backgrounds are treated as fully uncorrelated across n_{jet} and n_{b} categories and H_{T} bins, and with respect to the "normalisation" systematic uncertainties summarised in Table 2.

6 Results

A likelihood model of the observations in all data samples is used to obtain a consistent prediction of the SM backgrounds and to test for the presence of a variety of signal models. In each bin of H_T for events in the same category of n_{jet} and n_b, the observation is modelled as a Poisson-distributed variable around the sum of the SM expectation and a potential signal contribution (assumed to be zero in the following discussion). The SM expectation is related to the expected yields in the μ + jets, $\mu\mu$ + jets, and γ + jets control samples via transfer factors derived from simulation. Likelihood functions describe the yields in the H_T bins of the μ + jets, $\mu\mu$ + jets, and γ + jets control samples in the same category of n_{jet} and n_b as the signal region. The systematic uncertainties summarised in Table 2 are accommodated in the likelihood function by nuisance parameters, the measurements of which are assumed to follow a log-normal distribution. In the presence of a non-zero signal contribution, the CL_s technique [38, 39] is used to determine upper limits on production cross section using asymptotic formulae.

The expected number of events from SM processes is determined from a simultaneous fit to the signal region and up to three control samples. The likelihood function is maximised over all fit parameters under the SM-only hypothesis. Tables 3–5 summarise the observed yields and "pre-fit" and "post-fit" SM expectations for signal candidate events in the monojet, asymmetric, and symmetric categories, respectively. No significant tension is observed between the predictions and data in the signal region, which is well described by the SM-only hypothesis.

Table 3: Observed data counts and "post-fit" background expectations based on the result of a combined fit to the signal region and multiple control regions under the SM-only hypothesis for the monojet event category. The rows labelled SM "pre-fit" show the background expectations when excluding the signal region from the fit. The uncertainties include statistical as well as systematic contributions.

		H_T (GeV)							
	(n_{jet}, n_b)	200-250	250-300	300-350	350-400	400-500	500-600	600-800	800-∞
Data	(1, 0)	11433	3758	1375	635	447	115	49	–
SM post-fit	(1, 0)	11410.9 ± 115.4	3752.7 ± 67.9	1368.0 ± 35.7	627.3 ± 22.7	442.4 ± 22.3	115.7 ± 9.5	49.1 ± 6.6	–
SM pre-fit	(1, 0)	10615.5 ± 555.1	3606.7 ± 334.4	1315.4 ± 103.0	539.4 ± 72.6	405.0 ± 51.6	118.6 ± 22.9	49.5 ± 19.1	–
Data	(1, 1)	410	139	51	25	23	5	–	–
SM post-fit	(1, 1)	415.9 ± 17.3	140.2 ± 10.2	51.6 ± 6.0	23.2 ± 4.4	19.8 ± 3.2	4.4 ± 1.5	–	–
SM pre-fit	(1, 1)	436.1 ± 39.9	143.6 ± 22.9	52.9 ± 11.9	19.8 ± 6.2	16.9 ± 4.1	3.9 ± 2.3	–	–

Table 4: Observed data counts and "post-fit" background expectations based on the result of a combined fit to the signal region and multiple control regions under the SM-only hypothesis for the "asymmetric" event categories. The rows labelled SM "pre-fit" show the background expectations when excluding the signal region from the fit. The uncertainties include statistical as well as systematic contributions.

		H_T (GeV)							
	(n_{jet}, n_b)	200-250	250-300	300-350	350-400	400-500	500-600	600-800	800-∞
Data	(2a, 0)	4831	1396	512	214	131	24	16	–
SM post-fit	(2a, 0)	4834.3 ± 89.3	1398.3 ± 48.5	512.2 ± 22.6	210.6 ± 13.8	130.3 ± 9.1	27.5 ± 4.2	16.1 ± 3.2	–
SM pre-fit	(2a, 0)	4634.3 ± 533.6	1412.9 ± 113.8	515.3 ± 55.2	193.1 ± 37.4	132.4 ± 20.5	32.7 ± 8.3	16.3 ± 6.6	–
Data	(2a, 1)	431	124	44	15	7	4	–	–
SM post-fit	(2a, 1)	421.4 ± 18.1	125.4 ± 9.0	42.5 ± 4.2	16.9 ± 2.8	9.6 ± 1.5	3.5 ± 1.1	–	–
SM pre-fit	(2a, 1)	372.5 ± 48.7	126.5 ± 12.3	41.8 ± 5.9	17.9 ± 4.3	10.6 ± 2.3	3.6 ± 1.6	–	–
Data	(2a, 2)	26	10	2	1	0	–	–	–
SM post-fit	(2a, 2)	24.3 ± 3.1	5.9 ± 1.2	4.3 ± 1.1	1.4 ± 0.5	0.6 ± 0.4	–	–	–
SM pre-fit	(2a, 2)	21.9 ± 4.1	4.8 ± 1.4	5.0 ± 1.3	1.4 ± 0.7	0.7 ± 0.4	–	–	–
Data	(3a, 0)	1271	1336	647	218	90	15	9	–
SM post-fit	(3a, 0)	1271.0 ± 34.2	1313.0 ± 31.7	642.2 ± 26.5	222.0 ± 18.7	91.1 ± 9.0	15.2 ± 3.8	8.8 ± 2.9	–
SM pre-fit	(3a, 0)	1187.9 ± 165.2	1159.2 ± 103.7	582.2 ± 72.8	220.6 ± 33.7	94.9 ± 20.0	16.3 ± 6.6	8.5 ± 5.4	–
Data	(3a, 1)	256	226	123	50	12	1	1	–
SM post-fit	(3a, 1)	250.9 ± 14.1	238.6 ± 12.3	116.4 ± 8.5	40.9 ± 4.8	11.1 ± 1.9	1.9 ± 0.6	1.1 ± 0.7	–
SM pre-fit	(3a, 1)	217.7 ± 32.0	248.4 ± 24.3	98.4 ± 15.6	32.3 ± 6.0	10.7 ± 2.6	2.1 ± 0.8	1.1 ± 1.0	–
Data	(3a, 2)	45	45	20	9	1	0	–	–
SM post-fit	(3a, 2)	42.8 ± 5.1	43.5 ± 4.0	22.4 ± 3.0	9.5 ± 1.7	1.3 ± 0.4	0.3 ± 0.2	–	–
SM pre-fit	(3a, 2)	38.2 ± 6.9	41.1 ± 5.5	23.0 ± 4.6	9.1 ± 2.2	1.4 ± 0.6	0.4 ± 0.3	–	–
Data	(3a, $\geq$ 3)	3	1	1	–	–	–	–	–
SM post-fit	(3a, $\geq$ 3)	1.1 ± 0.5	1.2 ± 0.6	0.5 ± 0.4	–	–	–	–	–
SM pre-fit	(3a, $\geq$ 3)	0.5 ± 0.5	1.1 ± 0.6	0.2 ± 0.4	–	–	–	–	–
Data	(4a, 0)	3	139	319	211	105	15	2	–
SM post-fit	(4a, 0)	2.1 ± 0.8	135.5 ± 11.3	316.0 ± 14.9	211.9 ± 14.4	104.8 ± 9.4	13.7 ± 3.2	2.1 ± 0.6	–
SM pre-fit	(4a, 0)	1.8 ± 0.8	119.1 ± 21.6	285.6 ± 35.3	204.1 ± 30.7	102.7 ± 22.0	12.5 ± 4.1	2.2 ± 0.8	–
Data	(4a, 1)	1	47	151	81	45	3	0	–
SM post-fit	(4a, 1)	0.9 ± 0.4	40.6 ± 4.8	136.1 ± 10.0	76.0 ± 7.3	41.7 ± 5.0	3.3 ± 1.0	0.5 ± 0.2	–
SM pre-fit	(4a, 1)	0.9 ± 0.4	31.0 ± 7.0	105.4 ± 14.2	66.7 ± 12.8	38.1 ± 7.5	3.3 ± 1.0	0.5 ± 0.2	–
Data	(4a, 2)	0	10	36	22	6	0	0	–
SM post-fit	(4a, 2)	0.2 ± 0.2	10.8 ± 2.0	35.9 ± 4.4	23.0 ± 2.9	8.7 ± 1.4	0.5 ± 0.3	0.1 ± 0.1	–
SM pre-fit	(4a, 2)	0.1 ± 0.2	10.9 ± 2.4	33.4 ± 5.2	22.5 ± 5.4	9.5 ± 2.3	0.5 ± 0.2	0.1 ± 0.1	–
Data	(4a, $\geq$ 3)	–	0	0	2	2	–	–	–
SM post-fit	(4a, $\geq$ 3)	–	0.6 ± 0.5	2.2 ± 0.9	1.3 ± 0.6	1.4 ± 0.7	–	–	–
SM pre-fit	(4a, $\geq$ 3)	–	0.6 ± 0.6	2.9 ± 1.3	1.0 ± 0.7	1.2 ± 0.7	–	–	–
Data	($\geq$ 5a, 0)	–	1	30	79	91	19	3	–
SM post-fit	($\geq$ 5a, 0)	–	1.1 ± 1.5	28.9 ± 4.5	80.7 ± 7.7	90.6 ± 8.2	18.2 ± 4.1	4.4 ± 1.4	–
SM pre-fit	($\geq$ 5a, 0)	–	0.0 ± 3.4	26.5 ± 7.9	80.0 ± 16.4	86.4 ± 13.9	17.8 ± 7.6	6.8 ± 1.9	–
Data	($\geq$ 5a, 1)	–	0	19	47	58	10	0	–
SM post-fit	($\geq$ 5a, 1)	–	0.7 ± 0.5	18.3 ± 3.2	42.1 ± 5.4	55.8 ± 5.5	11.3 ± 2.4	2.1 ± 0.8	–
SM pre-fit	($\geq$ 5a, 1)	–	0.8 ± 1.1	17.1 ± 4.8	32.0 ± 7.4	50.4 ± 10.5	12.9 ± 4.4	3.3 ± 0.8	–
Data	($\geq$ 5a, 2)	–	0	9	22	23	4	1	–
SM post-fit	($\geq$ 5a, 2)	–	0.0 ± 0.0	5.9 ± 1.6	20.5 ± 3.6	21.2 ± 3.5	4.5 ± 1.2	0.9 ± 0.4	–
SM pre-fit	($\geq$ 5a, 2)	–	0.0 ± 0.0	4.0 ± 1.7	17.7 ± 5.0	18.9 ± 4.7	4.8 ± 2.1	1.3 ± 0.4	–
Data	($\geq$ 5a, $\geq$ 3)	–	–	0	2	3	0	–	–
SM post-fit	($\geq$ 5a, $\geq$ 3)	–	–	0.4 ± 0.3	1.7 ± 0.8	3.3 ± 1.0	0.4 ± 0.4	–	–
SM pre-fit	($\geq$ 5a, $\geq$ 3)	–	–	0.2 ± 0.5	1.3 ± 1.1	3.3 ± 1.5	0.4 ± 0.4	–	–

Table 5: Observed data counts and "post-fit" background expectations based on the result of a combined fit to the signal region and multiple control regions under the SM-only hypothesis for the "symmetric" event categories. The rows labelled SM "pre-fit" show the background expectations when excluding the signal region from the fit. The uncertainties include statistical as well as systematic contributions.

		H_T (GeV)							
	(n_{jet}, n_b)	200-250	250-300	300-350	350-400	400-500	500-600	600-800	800-∞
Data	(2, 0)	968	997	657	398	301	110	56	49
SM post-fit	(2, 0)	969.9 ± 51.2	996.4 ± 36.2	656.8 ± 25.1	395.5 ± 18.7	312.3 ± 16.4	107.3 ± 10.6	53.1 ± 6.2	47.2 ± 6.4
SM pre-fit	(2, 0)	943.9 ± 134.2	938.4 ± 148.4	627.9 ± 86.0	341.4 ± 61.3	329.1 ± 38.4	105.2 ± 24.3	43.8 ± 12.2	44.4 ± 11.4
Data	(2, 1)	111	100	65	37	35	5	4	2
SM post-fit	(2, 1)	104.2 ± 9.5	87.1 ± 8.1	54.9 ± 6.0	33.4 ± 4.4	26.4 ± 2.8	8.1 ± 1.6	4.2 ± 1.2	3.4 ± 0.9
SM pre-fit	(2, 1)	80.9 ± 16.0	57.9 ± 11.1	40.8 ± 7.3	26.8 ± 5.7	24.1 ± 3.7	9.5 ± 2.7	4.0 ± 1.4	3.7 ± 1.3
Data	(2, 2)	7	4	2	3	3	0	0	–
SM post-fit	(2, 2)	4.6 ± 1.8	2.7 ± 1.2	3.0 ± 1.3	1.5 ± 0.7	1.4 ± 0.4	1.0 ± 0.5	0.2 ± 0.2	–
SM pre-fit	(2, 2)	1.1 ± 2.3	0.8 ± 1.9	3.4 ± 2.0	0.7 ± 0.8	1.1 ± 0.5	1.3 ± 0.8	0.2 ± 0.2	–
Data	(3, 0)	2	176	505	491	547	185	90	72
SM post-fit	(3, 0)	1.4 ± 1.4	175.8 ± 13.3	504.3 ± 26.5	484.8 ± 20.5	541.3 ± 24.0	189.0 ± 15.3	89.9 ± 8.2	71.0 ± 7.2
SM pre-fit	(3, 0)	0.0 ± 2.4	173.6 ± 26.2	491.8 ± 63.6	421.9 ± 58.6	499.2 ± 65.1	195.4 ± 36.8	89.5 ± 23.7	68.0 ± 11.6
Data	(3, 1)	–	38	90	100	76	30	15	10
SM post-fit	(3, 1)	–	38.1 ± 4.1	82.0 ± 7.4	93.7 ± 7.0	79.3 ± 6.8	27.3 ± 3.6	15.2 ± 2.8	9.6 ± 1.6
SM pre-fit	(3, 1)	–	37.9 ± 6.3	70.5 ± 11.1	81.2 ± 11.9	79.2 ± 11.6	26.4 ± 5.9	15.3 ± 4.1	9.2 ± 2.0
Data	(3, 2)	–	10	10	10	13	5	1	1
SM post-fit	(3, 2)	–	6.9 ± 1.5	15.3 ± 2.3	15.8 ± 2.1	12.0 ± 1.8	3.6 ± 0.7	0.8 ± 0.3	1.0 ± 0.3
SM pre-fit	(3, 2)	–	5.9 ± 1.7	17.5 ± 3.2	16.4 ± 3.0	11.3 ± 2.2	3.4 ± 1.0	0.8 ± 0.3	0.9 ± 0.3
Data	$(3, \geq 3)$	–	0	–	–	1	–	–	–
SM post-fit	$(3, \geq 3)$	–	0.1 ± 0.2	–	–	0.5 ± 0.2	–	–	–
SM pre-fit	$(3, \geq 3)$	–	0.0 ± 0.3	–	–	0.4 ± 0.2	–	–	–
Data	(4, 0)	–	–	60	148	308	157	104	60
SM post-fit	(4, 0)	–	–	57.4 ± 7.5	149.5 ± 14.3	309.1 ± 16.5	156.9 ± 12.4	102.2 ± 9.6	56.6 ± 6.2
SM pre-fit	(4, 0)	–	–	48.8 ± 14.1	163.1 ± 65.7	301.0 ± 46.9	155.8 ± 36.3	96.5 ± 19.1	52.8 ± 11.3
Data	(4, 1)	–	–	12	72	101	31	15	9
SM post-fit	(4, 1)	–	–	15.3 ± 2.7	71.5 ± 8.5	94.5 ± 7.6	34.2 ± 4.3	18.1 ± 2.6	11.3 ± 1.8
SM pre-fit	(4, 1)	–	–	19.9 ± 6.3	67.1 ± 19.0	84.6 ± 11.7	36.9 ± 8.3	18.4 ± 4.3	11.6 ± 2.5
Data	(4, 2)	–	–	6	24	34	11	6	2
SM post-fit	(4, 2)	–	–	4.6 ± 1.5	21.6 ± 3.8	33.5 ± 3.8	8.1 ± 1.6	3.1 ± 0.6	2.1 ± 0.5
SM pre-fit	(4, 2)	–	–	3.6 ± 2.0	17.2 ± 5.8	31.9 ± 5.0	7.3 ± 2.1	2.8 ± 0.7	2.1 ± 0.6
Data	$(4, \geq 3)$	–	–	0	3	0	1	0	0
SM post-fit	$(4, \geq 3)$	–	–	0.2 ± 0.3	2.1 ± 0.9	1.2 ± 0.6	0.7 ± 0.3	0.1 ± 0.1	0.1 ± 0.0
SM pre-fit	$(4, \geq 3)$	–	–	0.0 ± 0.4	1.5 ± 1.1	1.5 ± 0.8	0.6 ± 0.4	0.0 ± 0.1	0.0 ± 0.0
Data	$(\geq 5, 0)$	–	–	–	7	89	84	75	59
SM post-fit	$(\geq 5, 0)$	–	–	–	10.3 ± 2.6	88.1 ± 9.1	81.3 ± 8.2	74.4 ± 7.0	58.3 ± 6.6
SM pre-fit	$(\geq 5, 0)$	–	–	–	15.3 ± 5.9	86.1 ± 13.1	78.1 ± 20.0	71.0 ± 14.4	46.2 ± 12.8
Data	$(\geq 5, 1)$	–	–	–	4	42	39	31	21
SM post-fit	$(\geq 5, 1)$	–	–	–	3.0 ± 1.0	43.3 ± 5.0	38.9 ± 4.6	27.8 ± 3.2	20.0 ± 3.3
SM pre-fit	$(\geq 5, 1)$	–	–	–	2.5 ± 1.5	44.1 ± 8.0	38.9 ± 8.7	25.3 ± 5.6	15.8 ± 3.5
Data	$(\geq 5, 2)$	–	–	–	0	22	12	7	12
SM post-fit	$(\geq 5, 2)$	–	–	–	1.4 ± 0.8	20.1 ± 3.2	14.6 ± 2.3	7.7 ± 1.2	6.6 ± 1.3
SM pre-fit	$(\geq 5, 2)$	–	–	–	2.1 ± 1.3	18.8 ± 4.1	15.4 ± 3.8	7.6 ± 1.9	4.6 ± 1.2
Data	$(\geq 5, \geq 3)$	–	–	–	–	0	1	0	3
SM post-fit	$(\geq 5, \geq 3)$	–	–	–	–	0.7 ± 0.5	1.2 ± 0.5	1.3 ± 0.4	1.1 ± 0.4
SM pre-fit	$(\geq 5, \geq 3)$	–	–	–	–	0.7 ± 0.7	1.2 ± 0.7	1.4 ± 0.5	0.8 ± 0.3

7 Interpretation

The results of this search are interpreted in terms of upper limits in the production cross section as a function of the parent sparticle and LSP mass for simplified models [18–20] that represent the pair production of gluinos and their subsequent decays to four quarks and two LSPs. The event samples for the simplified models are generated with MADGRAPH V5 [32]. Inclusive, process-dependent, NLO calculations of SUSY production cross sections, with next-to-leading-logarithmic (NLL) corrections, are obtained with the program PROSPINO [40–45]. The samples are generated using the CTEQ6L1 [35] PDFs. The distribution of the number of pp interactions per bunch crossing for the simulated samples matches that observed in data. Various uncertainties in the experimental acceptance are considered, for which typical magnitudes are summarised in Table 6.

Table 6: Typical magnitudes of systematic uncertainties in the experimental acceptance for the signal models considered.

Systematic source	Type	Correlated	Typical magnitude (%)
Luminosity	Normalisation	Yes	4.6
Monte Carlo statistics	Norm. + shape	No	1–50
Initial state radiation	Norm. + shape	Yes	0–30
Jet energy scale	Norm. + shape	Yes	3–10
Pile-up	Norm. + shape	Yes	0-5
Trigger	Norm. + shape	Yes	0–10
Parton density functions	Normalisation	No	10
b-tag scale factors	Norm. + shape	Yes	5–30
Lepton scale factors	Normalisation	Yes	<5

Figure 3 shows for two categories in n_{jet} and n_{b} at high H_{T} that are expected to provide good sensitivity to gluino models the distribution of the data observations as a function of the $H_{\text{T}}^{\text{miss}}$ variable, the expected distribution for the sum of all SM background processes, and the expected distribution for an example benchmark signal model.

Figure 4 shows the observed upper limit on the production cross section at 95% confidence level (CL) as a function of the gluino and LSP masses for a range of simplified models assuming pair production of gluinos. The observed excluded regions are determined for gluino pair production assuming decoupled squarks. Also shown are the observed excluded regions when varying the production cross section by its theoretical uncertainty, and the expected excluded region with the ± 1 standard-deviation (σ) variations. The search places stringent limits in the mass parameter space, with observed exclusions in gluino and LSP masses as high as $\sim$1550 GeV and $\sim$950 GeV, respectively.

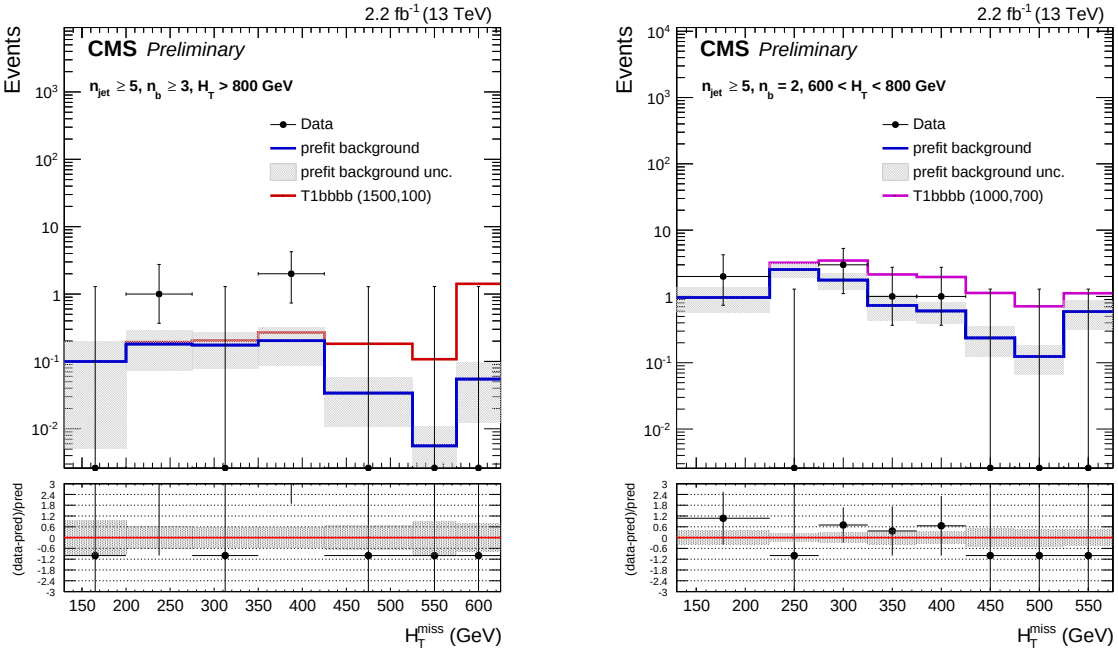

Figure 3: The $H_{\mathrm{T}}^{\mathrm{miss}}$ distribution observed in data and the expected distribution for the sum of all SM background processes in two representative event categories at high H_{T}. The expected distribution for an example benchmark model with a large (small) mass splitting between the gluino and LSP is also shown in the left (right) figure.

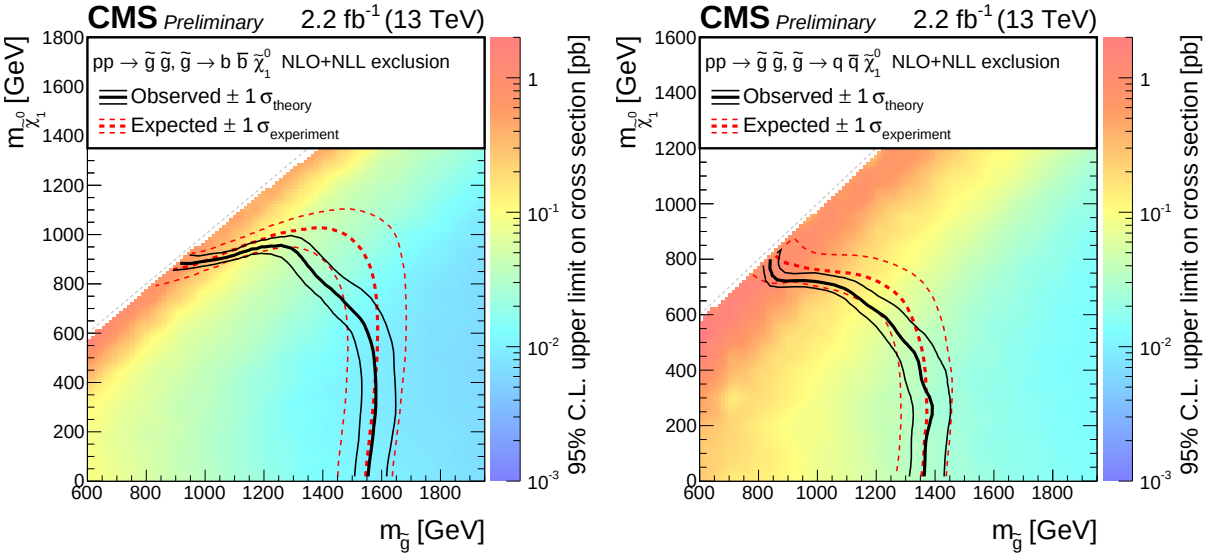

Figure 4: Observed upper limit in cross section at 95% CL (indicated by the colour scale) for simplified models that assume the pair production of gluinos, as a function of the gluino and $\tilde{\chi}_1^0$ masses for gluino three-body decays to $b\bar{b}\tilde{\chi}_1^0$ (left) and $q\bar{q}\tilde{\chi}_1^0$ (right). The black solid thick (thin) line indicates the observed mass exclusion region assuming the nominal ($\pm 1\sigma$ theory uncertainty) production cross section. The red dashed thick (thin) line indicates the median ($\pm 1\sigma$ experimental uncertainty) expected exclusion.

8 Summary

An inclusive search for supersymmetry with the CMS experiment is reported, based on a data sample of pp collisions collected at $\sqrt{s} = 13\,\text{TeV}$, corresponding to an integrated luminosity of $2.2 \pm 0.1\,\text{fb}^{-1}$. Final states with jets and significant $E_{\text{T}}^{\text{miss}}$, as expected from the production and decay of massive squarks and gluinos, have been analysed. The signal region is binned according to the number of reconstructed jets, the scalar and vector sums of the transverse momentum of jets, and the number of jets identified to originate from bottom quarks. The sum of standard model backgrounds per bin has been estimated from a simultaneous binned likelihood fit to event yields in the signal region and control samples. The observed yields in the signal region are found to be in agreement with the expected contributions from standard model processes. Limits are determined in the mass parameter space of simplified models of gluino pair-production assuming decoupled squarks. The excluded mass parameter space extends significantly beyond that set by previous searches at $\sqrt{s} = 8\,\text{TeV}$, with observed exclusions in gluino and LSP masses as high as $\sim$1550 GeV and $\sim$950 GeV, respectively.

References

[1] Y. A. Gol'fand and E. P. Likhtman, "Extension of the Algebra of Poincaré Group Generators and Violation of p Invariance", *JETP Lett.* **13** (1971) 323.

[2] J. Wess and B. Zumino, "Supergauge transformations in four dimensions", *Nucl. Phys. B* **70** (1974) 39, doi:10.1016/0550-3213(74)90355-1.

[3] H. P. Nilles, "Supersymmetry, Supergravity and Particle Physics", *Phys. Reports* **110** (1984) 1, doi:10.1016/0370-1573(84)90008-5.

[4] H. Haber and G. Kane, "The Search for Supersymmetry: Probing Physics Beyond the Standard Model", *Phys. Reports* **117** (1987) 75, doi:10.1016/0370-1573(85)90051-1.

[5] R. Barbieri, S. Ferrara, and C. A. Savoy, "Gauge Models with Spontaneously Broken Local Supersymmetry", *Phys. Lett. B* **119** (1982) 343, doi:10.1016/0370-2693(82)90685-2.

[6] S. Dawson, E. Eichten, and C. Quigg, "Search for Supersymmetric Particles in Hadron - Hadron Collisions", *Phys. Rev. D* **31** (1985) 1581, doi:10.1103/PhysRevD.31.1581.

[7] E. Witten, "Dynamical Breaking of Supersymmetry", *Nucl. Phys. B* **188** (1981) 513, doi:10.1016/0550-3213(81)90006-7.

[8] S. Dimopoulos and H. Georgi, "Softly Broken Supersymmetry and SU(5)", *Nucl. Phys. B* **193** (1981) 150, doi:10.1016/0550-3213(81)90522-8.

[9] ATLAS Collaboration, "Observation of a new particle in the search for the Standard Model Higgs boson with the ATLAS detector at the LHC", *Phys. Lett. B* **716** (2012) 1, doi:10.1016/j.physletb.2012.08.020.

[10] CMS Collaboration, "Observation of a new boson at a mass of 125 GeV with the CMS experiment at the LHC", *Phys. Lett. B* **716** (2012) 30, doi:10.1016/j.physletb.2012.08.021.

[11] G. R. Farrar and P. Fayet, "Phenomenology of the Production, Decay, and Detection of New Hadronic States Associated with Supersymmetry", *Phys. Lett. B* **76** (1978) 575, doi:10.1016/0370-2693(78)90858-4.

[12] CMS Collaboration, "CMS Luminosity Based on Pixel Cluster Counting - Summer 2012 Update", CMS Physics Analysis Summary CMS-PAS-LUM-12-001, 2012.

[13] CMS Collaboration, "Search for Supersymmetry in pp Collisions at 7 TeV in Events with Jets and Missing Transverse Energy", *Phys. Lett. B* **698** (2011) 196, doi:10.1016/j.physletb.2011.03.021.

[14] CMS Collaboration, "Search for Supersymmetry at the LHC in Events with Jets and Missing Transverse Energy", *Phys. Rev. Lett.* **107** (2011) 221804, doi:10.1103/PhysRevLett.107.221804.

[15] CMS Collaboration, "Search for supersymmetery in final states with missing transverse energy and 0, 1, 2, or $\geq$3 b-quark jets in 7 TeV pp collisions using the α_{T} variable", *JHEP* **01** (2013) 077, doi:10.1007/JHEP01(2013)077.

[16] CMS Collaboration, "Search for supersymmetry in hadronic final states with missing transverse energy using the variables α_T and b-quark multiplicity in pp collisions at $\sqrt{s} = 8$ TeV", *EPJC* **01** (2013) 077, doi:10.1007/JHEP01(2013)077.

[17] L. Randall and D. Tucker-Smith, "Dijet Searches for Supersymmetry at the Large Hadron Collider", *Phys. Rev. Lett.* **101** (2008) 221803, doi:10.1103/PhysRevLett.101.221803.

[18] J. Alwall, P. Schuster, and N. Toro, "Simplified Models for a First Characterization of New Physics at the LHC", *Phys. Rev. D* **79** (2009) 075020, doi:10.1103/PhysRevD.79.075020.

[19] J. Alwall, M.-P. Le, M. Lisanti, and J. G. Wacker, "Model-independent jets plus missing energy searches", *Phys. Rev. D* **79** (2009) 015005, doi:10.1103/PhysRevD.79.015005.

[20] D. Alves et al., "Simplified models for LHC new physics searches", *J. Phys. G* **39** (2012) 105005, doi:10.1088/0954-3899/39/10/105005.

[21] CMS Collaboration, "The CMS experiment at the CERN LHC", *JINST* **03** (2008) S08004, doi:10.1088/1748-0221/3/08/S08004.

[22] CMS Collaboration, "Electron reconstruction and identification at $\sqrt{s} = 7$ TeV", CMS Physics Analysis Summary EGM-10-004, 2010.

[23] CMS Collaboration, "Performance of CMS muon reconstruction in pp collision events at $\sqrt{s} = 7$ TeV", *JINST* **7** (2012) P10002, doi:10.1088/1748-0221/7/10/P10002.

[24] CMS Collaboration, "Isolated Photon Reconstruction and Identification at $\sqrt{s} = 7$ TeV", CMS Physics Analysis Summary EGM-10-006, 2010.

[25] CMS Collaboration, "Particle–Flow Event Reconstruction in CMS and Performance for Jets, Taus, and E_T^{miss}", CMS Physics Analysis Summary CMS-PAS-PFT-09-001, 2009.

[26] CMS Collaboration, "Commissioning of the particle-flow event reconstruction with the first LHC collisions recorded in the CMS detector", CMS Physics Analysis Summary CMS-PAS-PFT-10-001, 2010.

[27] M. Cacciari, G. P. Salam, and G. Soyez, "The anti-k_T jet clustering algorithm", *JHEP* **04** (2008) 063, doi:10.1088/1126-6708/2008/04/063.

[28] CMS Collaboration, "Determination of Jet Energy Calibration and Transverse Momentum Resolution in CMS", (2011). arXiv:1107.4277. Submitted to JHEP.

[29] CMS Collaboration, "Identification and filtering of uncharacteristic noise in the CMS hadron calorimeter", *JINST* **5** (2010) T03014, doi:10.1088/1748-0221/5/03/T03014.

[30] CMS Collaboration, "Electromagnetic calorimeter commissioning and first results with 7 TeV data", CMS Note CMS-NOTE-2010-012, 2010.

[31] CMS Collaboration, "Missing transverse energy performance of the CMS detector", *JINST* **6** (2011) P09001, doi:10.1088/1748-0221/6/09/P09001.

[32] J. Alwall et al., "MadGraph/MadEvent v4: The New Web Generation", *JHEP* **09** (2007) 028, arXiv:0706.2334.

[33] S. Frixione, P. Nason, and C. Oleari, "Matching NLO QCD computations with parton shower simulations: the POWHEG method", *JHEP* **11** (2007) 070, doi:10.1088/1126-6708/2007/11/070.

[34] T. Sjöstrand, S. Mrenna, and P. Z. Skands, "A Brief Introduction to PYTHIA 8.1", *Comput. Phys. Commun.* **178** (2008) 852, doi:10.1016/j.cpc.2008.01.036.

[35] J. Pumplin et al., "New generation of parton distributions with uncertainties from global QCD analysis", *JHEP* **07** (2002) 012, doi:10.1088/1126-6708/2002/07/012.

[36] S. Agostinelli et al., "GEANT4 — a simulation toolkit", *Nucl. Instr. and Meth. A* **506** (2003) 250, doi:10.1016/S0168-9002(03)01368-8.

[37] Z. Bern et al., "Driving Missing Data at Next-to-Leading Order", (2011). arXiv:1106.1423.

[38] A. L. Read, "Presentation of search results: the CL_s technique", *J. Phys. G* **28** (2002) 2693, doi:10.1088/0954-3899/28/10/313.

[39] G. Cowan, K. Cranmer, E. Gross, and O. Vitells, "Asymptotic formulae for likelihood-based tests of new physics", *Eur. Phys. J. C* **71** (2011) 1554, doi:10.1140/epjc/s10052-011-1554-0.

[40] W. Beenakker, R. Höpker, M. Spira, and P. M. Zerwas, "Squark and gluino production at hadron colliders", *Nucl. Phys. B* **492** (1997) 51, doi:10.1016/S0550-3213(97)00084-9.

[41] A. Kulesza and L. Motyka, "Soft gluon resummation for the production of gluino-gluino and squark-antisquark pairs at the LHC", *Phys. Rev. D* **80** (2009) 095004, doi:10.1103/PhysRevD.80.095004.

[42] A. Kulesza and L. Motyka, "Threshold Resummation for Squark-Antisquark and Gluino-Pair Production at the LHC", *Phys. Rev. Lett.* **102** (2009) 111802, doi:10.1103/PhysRevLett.102.111802.

[43] W. Beenakker et al., "Soft-gluon resummation for squark and gluino hadroproduction", *JHEP* **09** (2009) 041, doi:10.1088/1126-6708/2009/12/041.

[44] W. Beenakker et al., "Squark and gluino hadroproduction", *Int. J. Mod. Phys. A* **26** (2011) 2637, doi:10.1142/S0217751X11053560.

[45] M. Krämer et al., "Supersymmetry production cross sections in pp collisions at $\sqrt{s} = 7$ TeV", (2012). arXiv:1206.2892.